Electronic Supplementary Material (ESI) for Inorganic Chemistry Frontiers.

Supporting Information

A Water-stable Terbium Metal–Organic Framework as Highly Sensitive Fluorescent Sensor for Nitrite

Hui Min, Zongsu Han, Mengmeng Wang, Yongjie Li, Tianze Zhou, Wei Shi* and Peng Cheng*

Key Laboratory of Advanced Energy Materials Chemistry (MOE), College of Chemistry, Nankai University, Tianjin 300071, China.
E-mail: shiwei@nankai.edu.cn; pcheng@nankai.edu.cn.

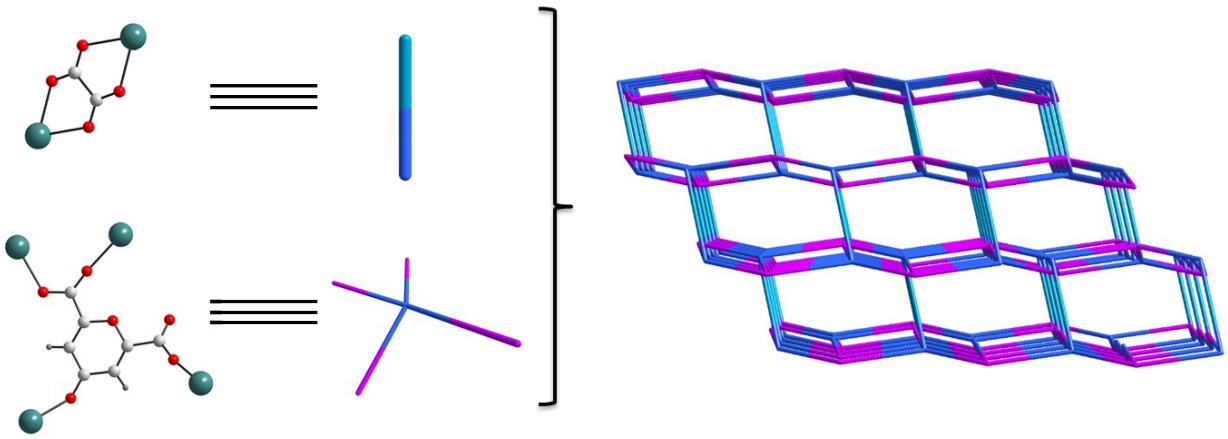

Fig. S1. The topology structure of Tb-MOF calculated by TOPOS-40.

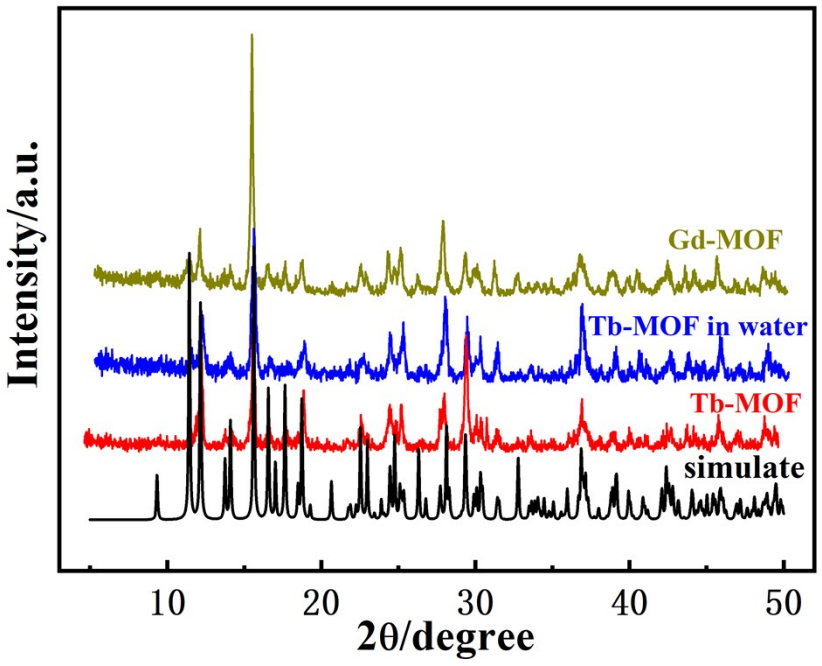

Fig. S2. The PXRD patterns of the Tb-MOF, the isomorphic Gd-MOF and the Tb-MOF immersed in water for 36 hours.

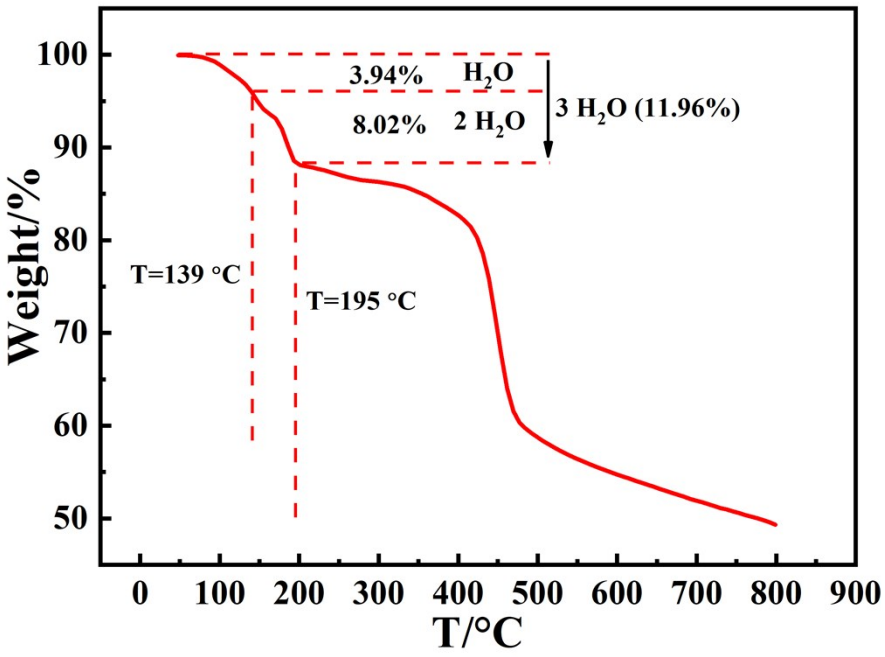

Fig. S3. The thermal gravimetric analyses (TGA) curve of Tb-MOF.

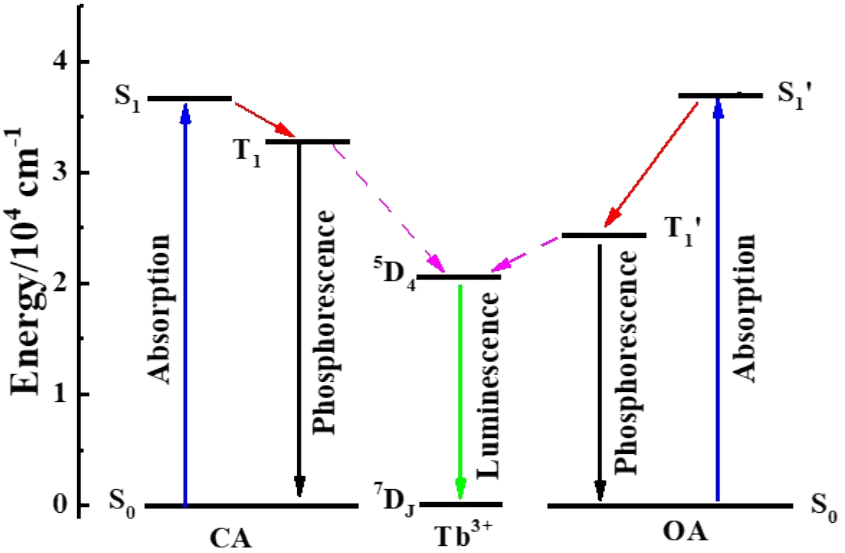

Fig. S4. The schematic energy transfer process in Tb-MOF.

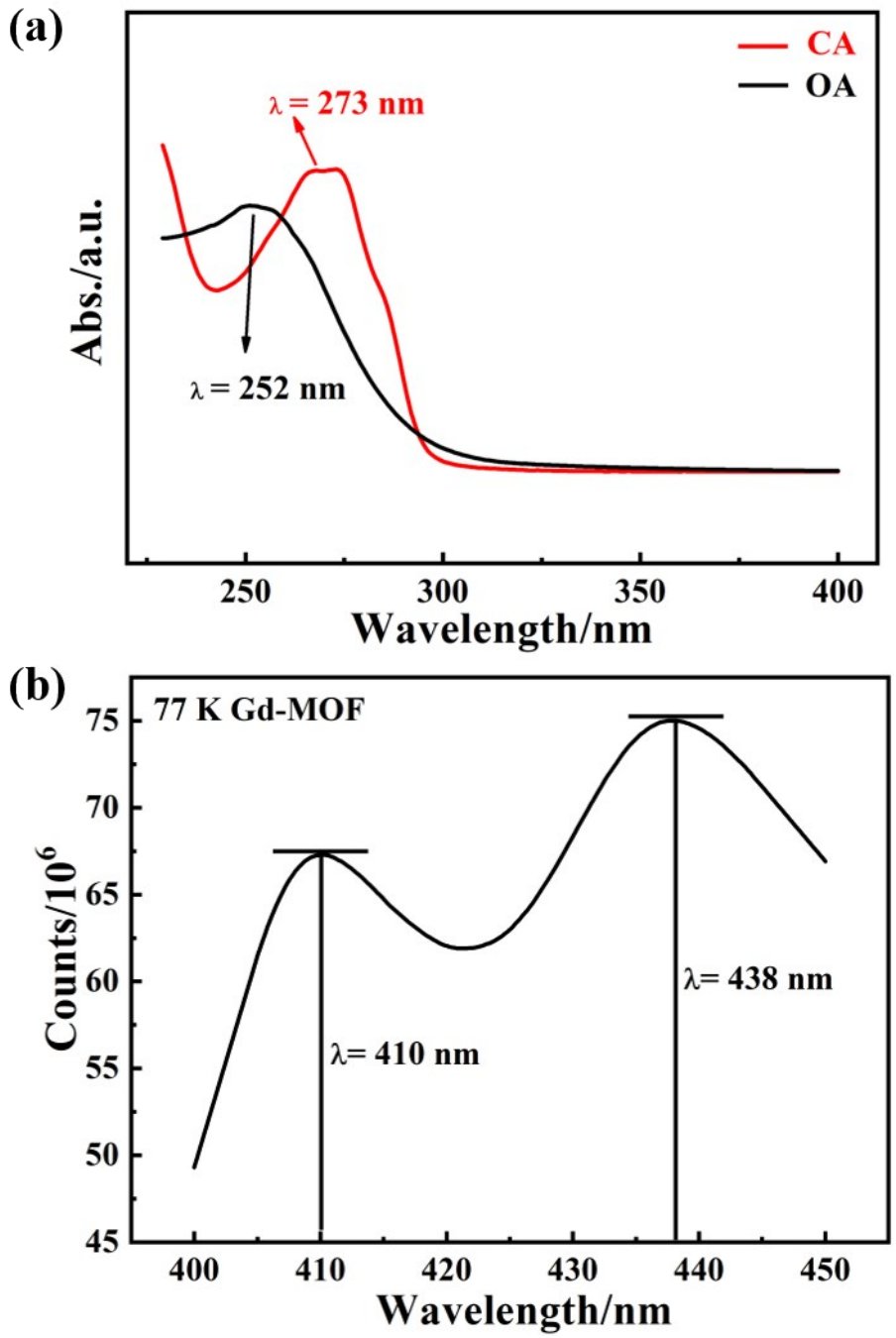

Fig. S5. (a) The UV-vis spectra of the ligands. (b) The 77 K phosphorescence spectrum of isomorphic Gd-MOF.

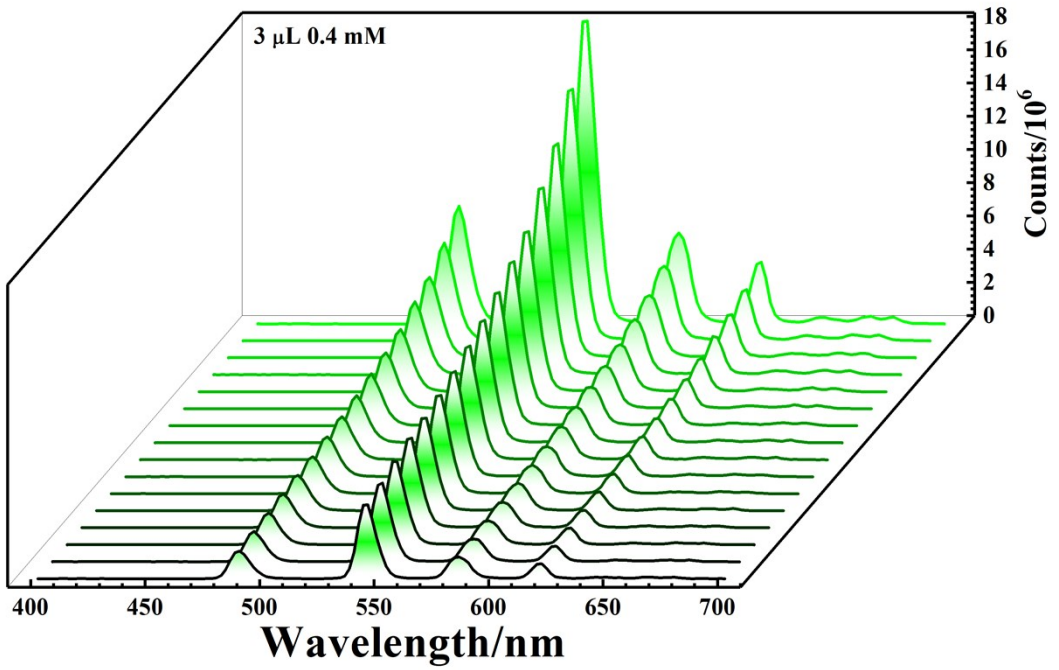

Fig. S6. The emission spectra of Tb-MOF in aqueous solution with different concentrations of $NaNO_2$ (Every time adding 3 uL 0.4 mM NO_2^-).

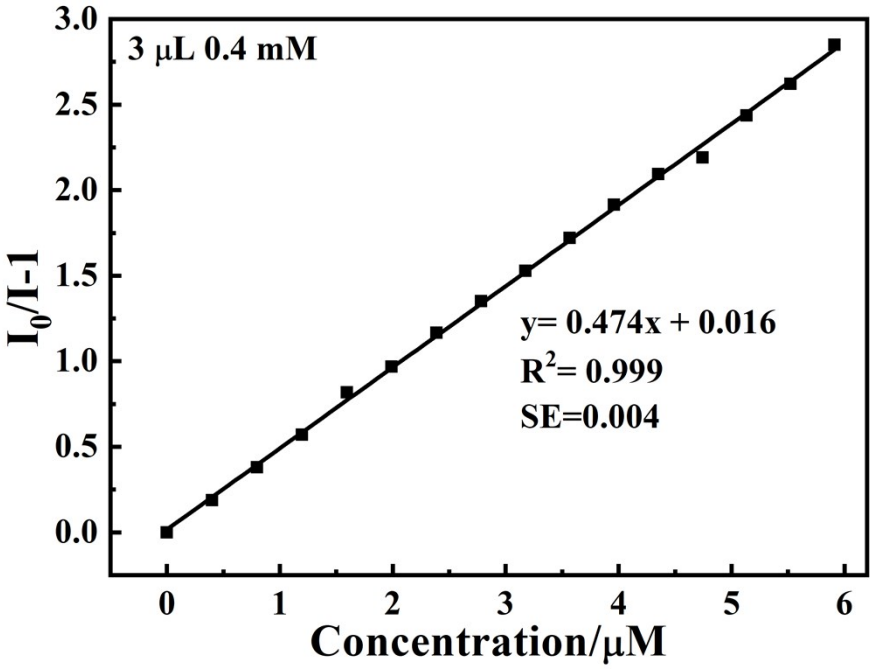

Fig. S7. The S−V plot of Tb-MOF in aqueous solution with different concentrations of $NaNO_2$.

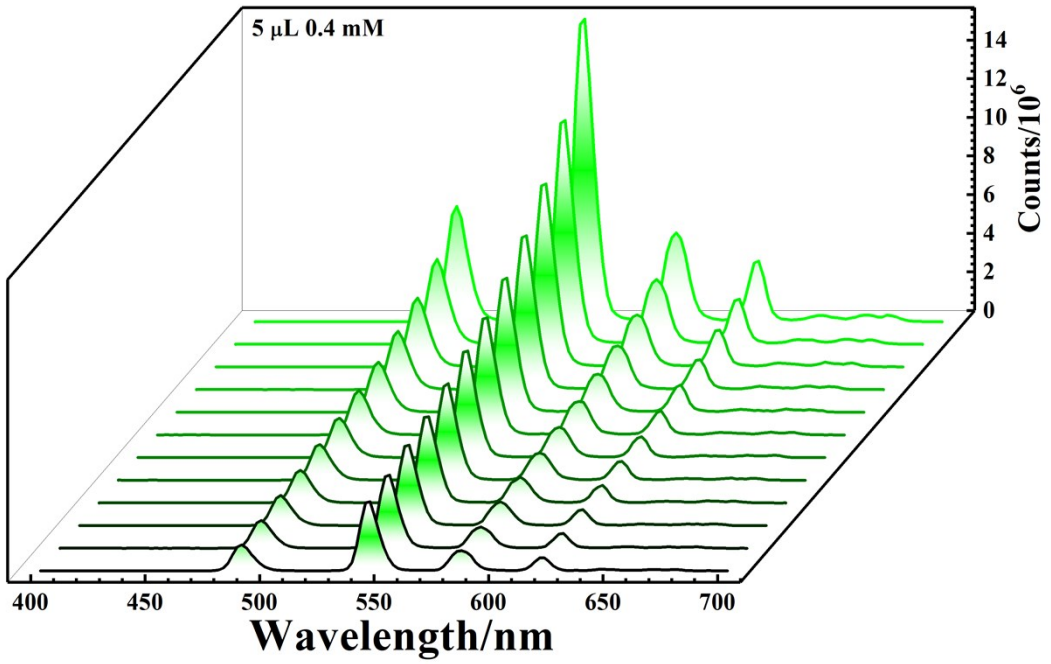

Fig. S8. The emission spectra of Tb-MOF in aqueous solution with different concentrations of $NaNO_2$ (Every time adding 5 uL 0.4 mM NO_2^-).

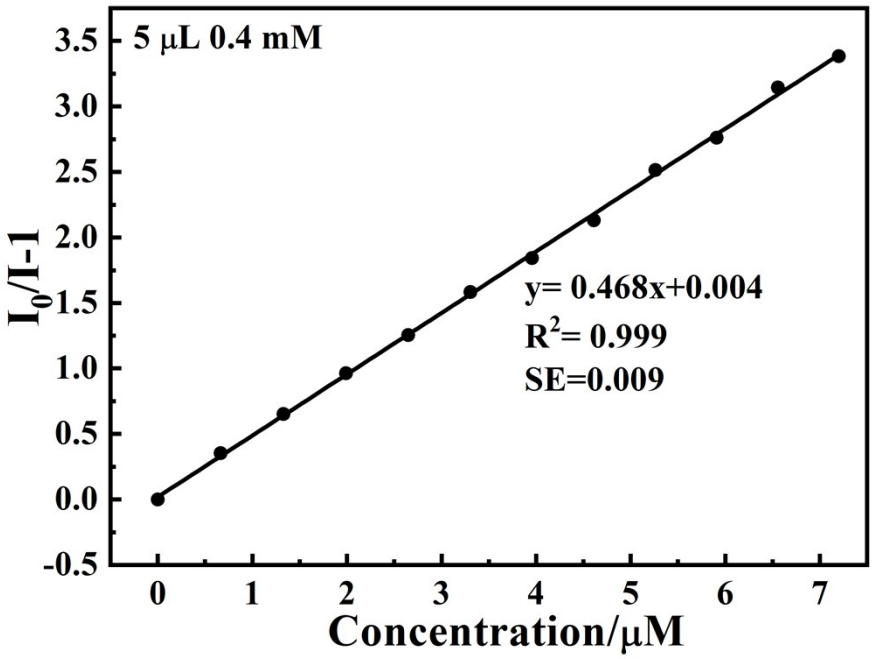

Fig. S9. The S−V plot of Tb-MOF in aqueous solution with different concentrations of $NaNO_2$.

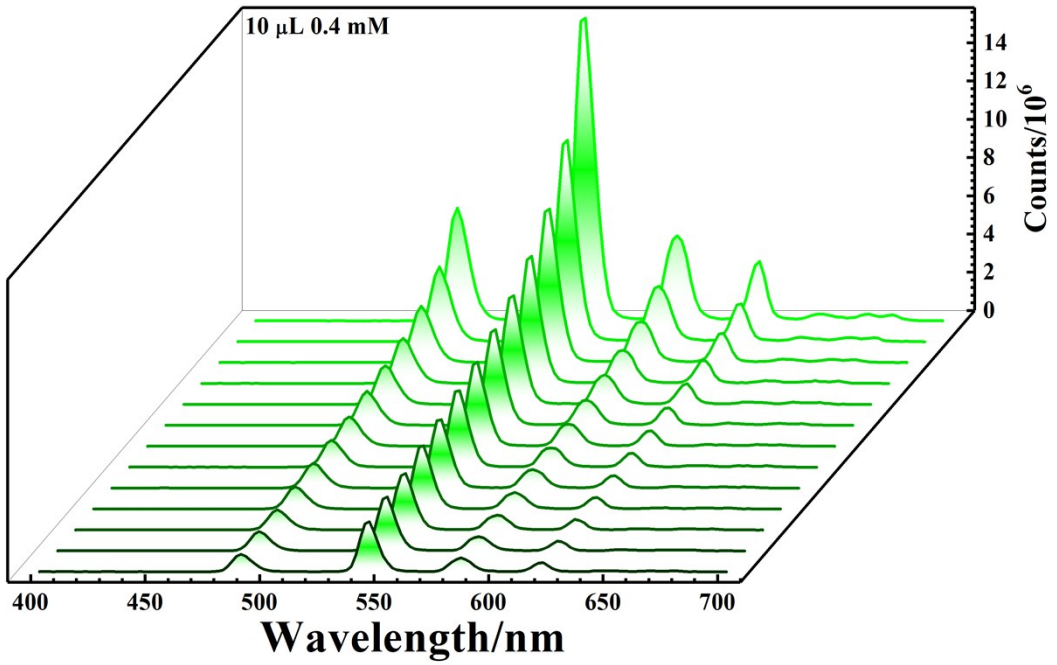

Fig. S10. The emission spectra of Tb-MOF in aqueous solution with different concentrations of $NaNO_2$ (Every time adding 10 uL 0.4 mM NO_2^-).

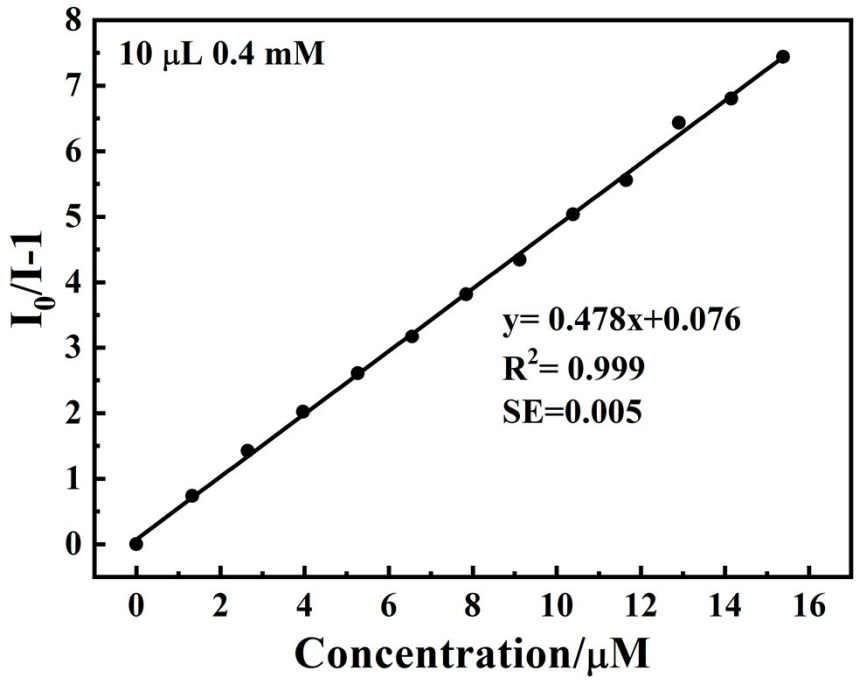

Fig. S11. The S−V plot of Tb-MOF in aqueous solution with different concentrations of $NaNO_2$.

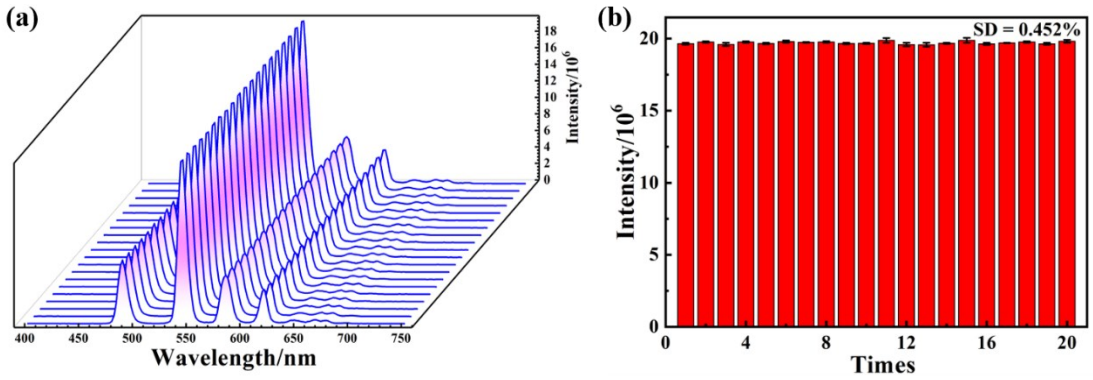

Fig. S12. The emission spectra (a) and the luminescent intensities (b) of Tb-MOF suspension with 20 consecutive tests without adding any species. SD is the standard deviation of luminescent intensities.

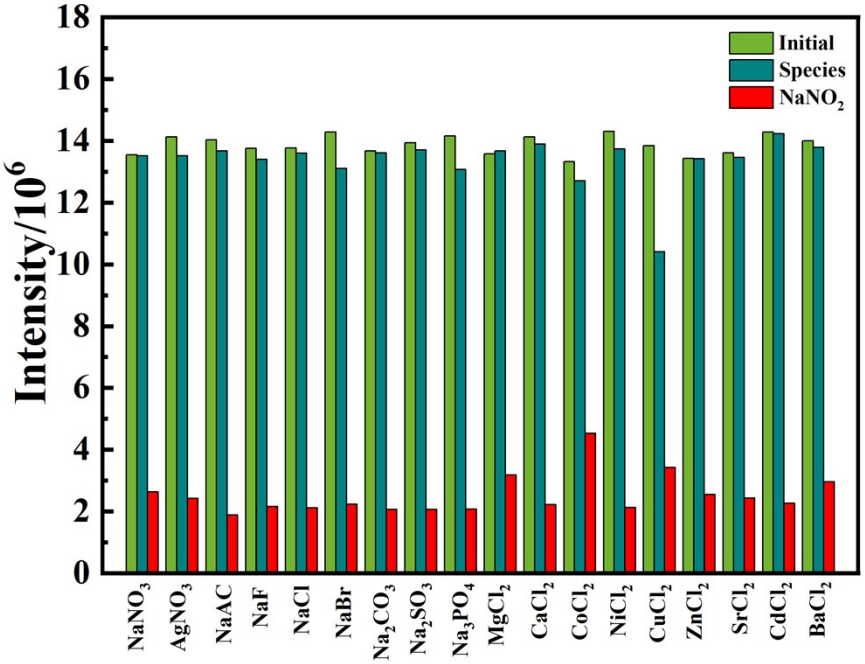

Fig. S13. The fluorescence intensities of Tb-MOF before and after adding 12 μM different species and $NaNO_2$.

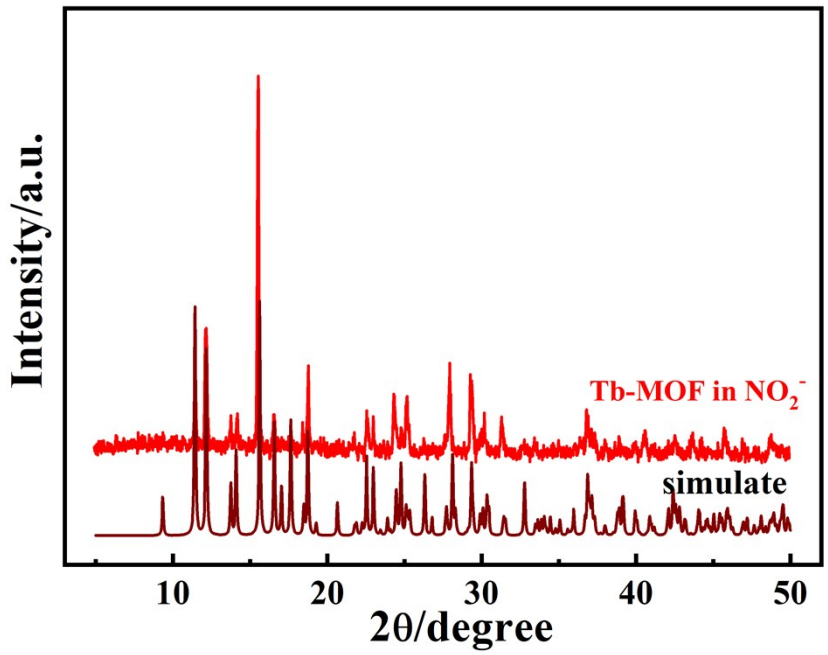

Fig. S14. The PXRD patterns of Tb-MOF immersed in 4 mM nitrite for 4 h.

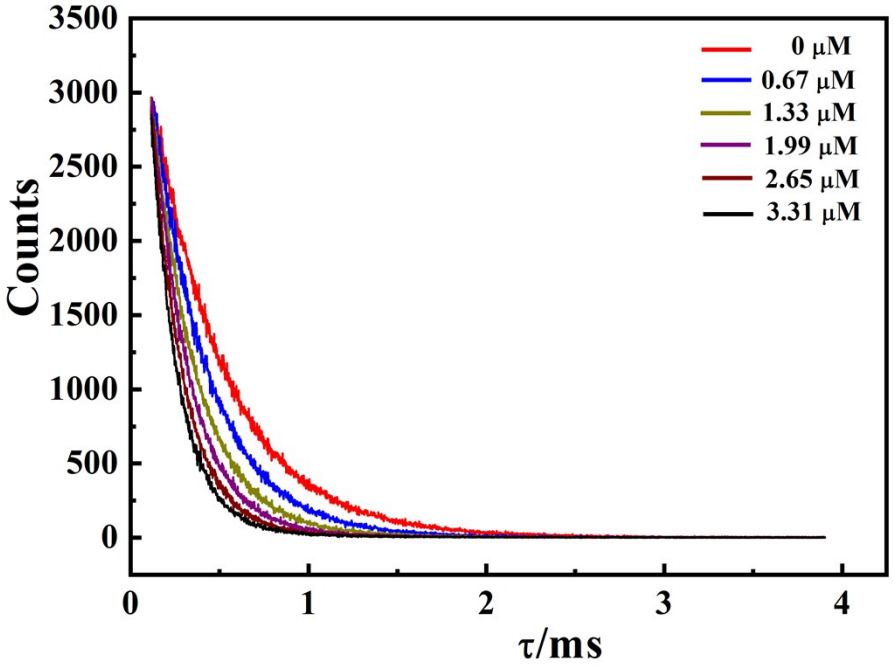

Fig. S15. The lifetimes of Tb-MOF before and after adding $NaNO_2$ with different concentrations.

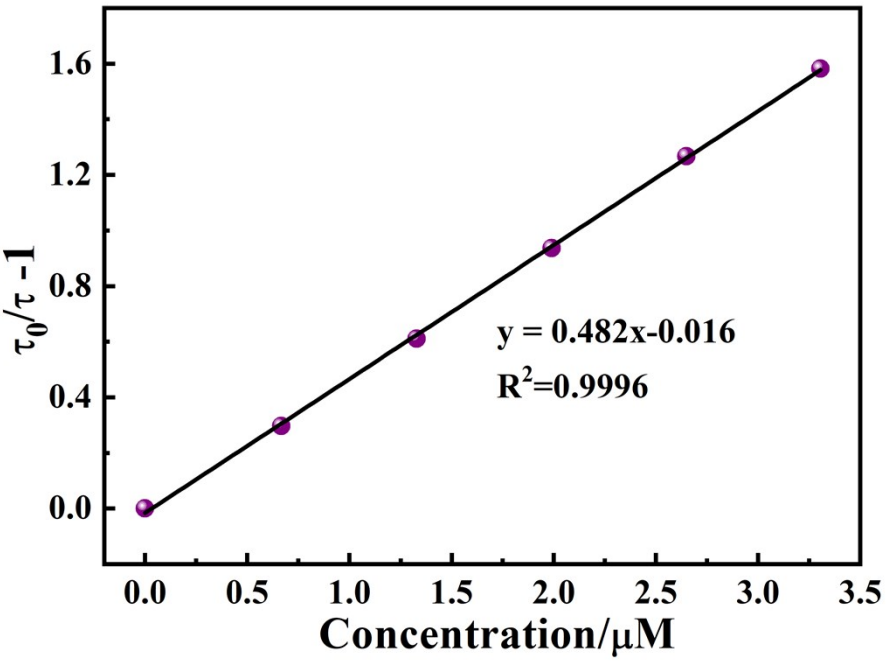

Fig. S16. The lifetime-based S−V plot of Tb-MOF in aqueous solution with different concentrations of $NaNO_2$.

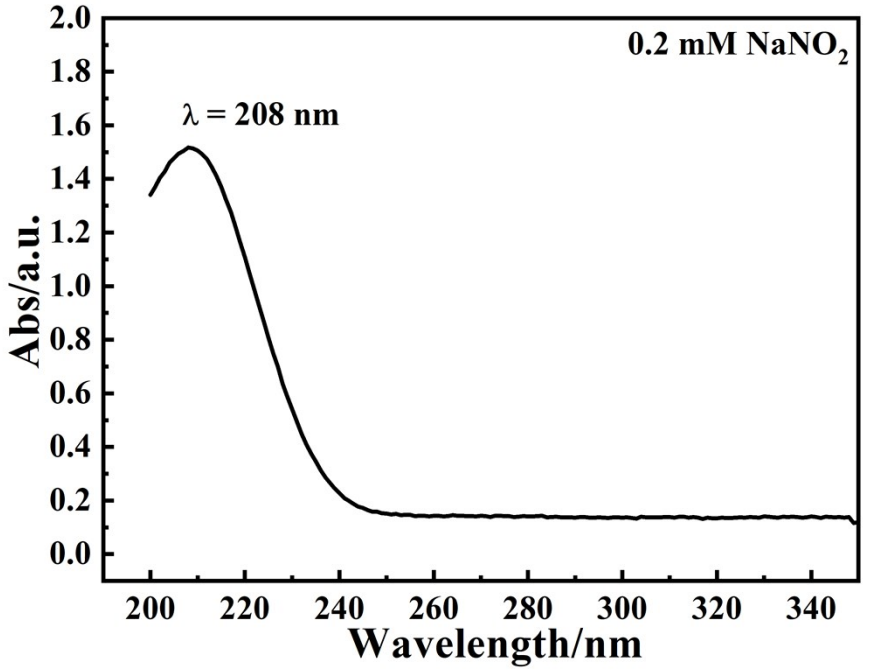

Fig. S17. The UV-vis spectrum of nitrite.

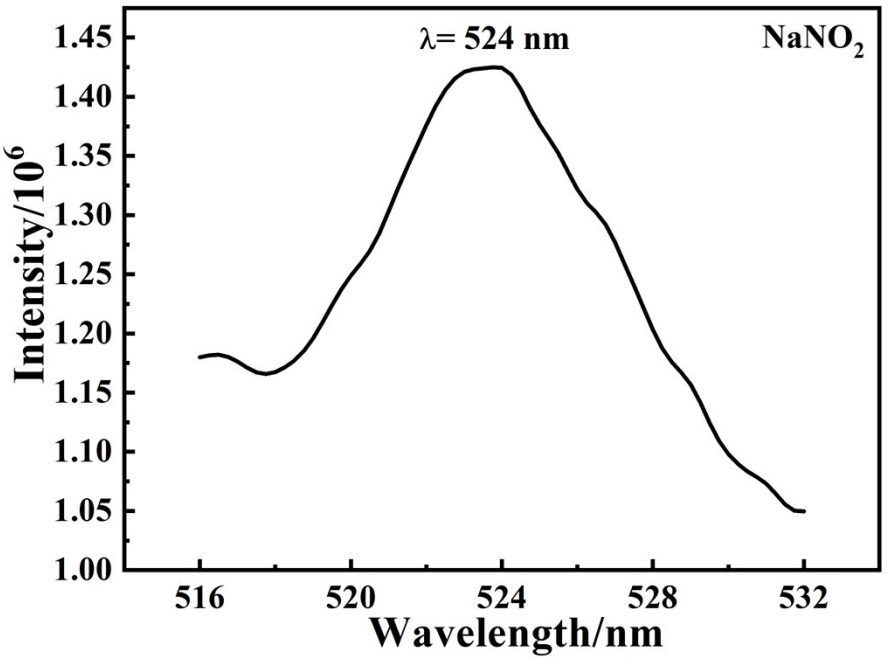

Fig. S18. The phosphorescence spectrum of nitrite at 77 K.

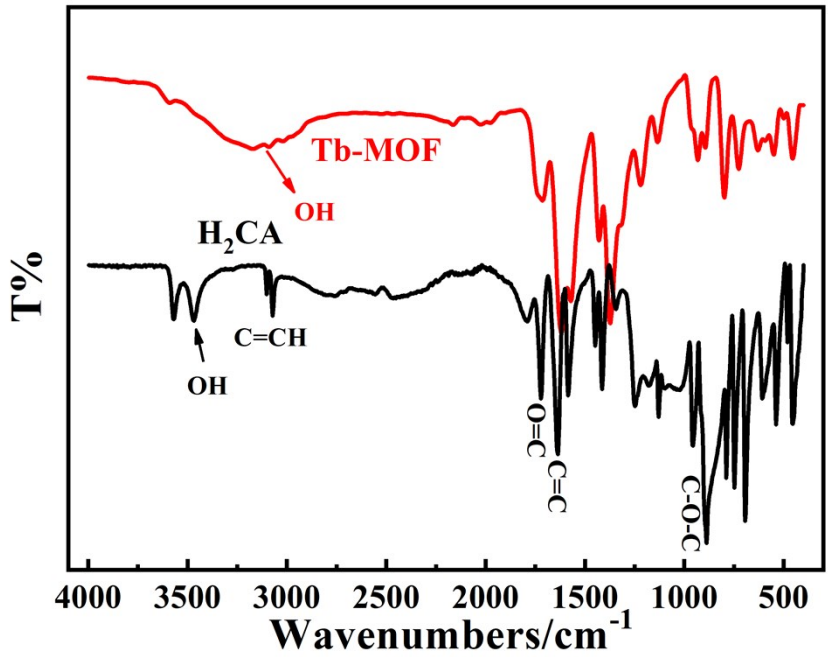

Fig. S19. The infrared spectra of H_2CA and Tb-MOF.

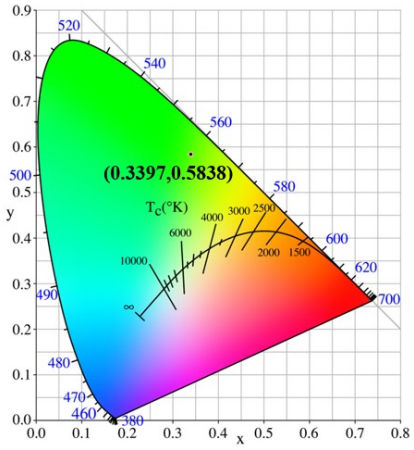

Fig. S20. The CIE-1931 chromaticity diagram of Tb-MOF.

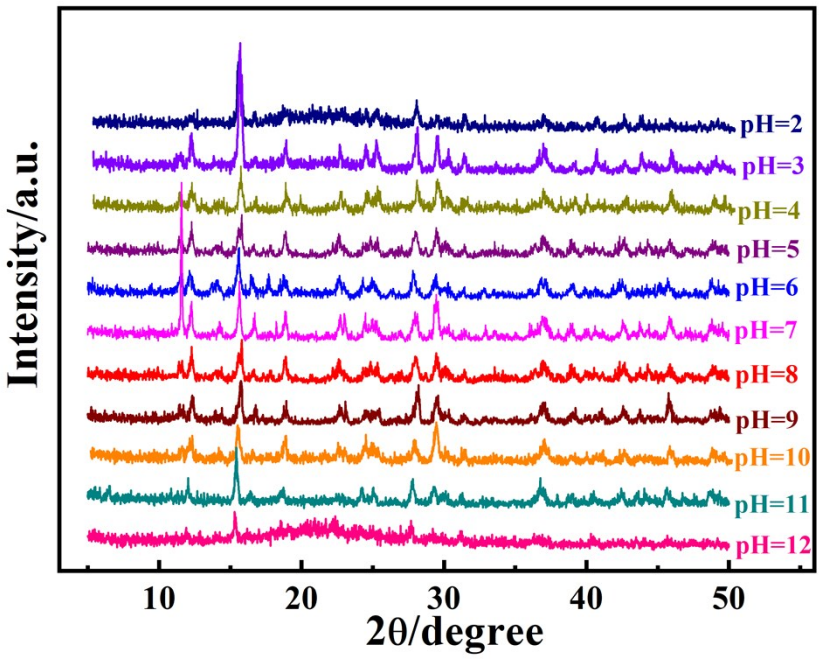

Fig. S21. The PXRD patterns of Tb-MOF immersed in aqueous solutions with different pH values.

Tb-MOF	
Formula	$C_8H_8O_{11}Tb$
Formula weight	439.06
T / K	120
λ / Å	0.71073
Crystal system	Triclinic
Space group	*P*-1
a / Å	7.6875(11)
b / Å	8.5576(13)
c / Å	10.0334(15)
α / deg	107.254(14)
β / deg	93.691(12)
γ / deg	106.819(13)
V / $Å^3$	595.19(16)
Z	2
ρcalc / g cm^{-3}	2.450
μ / mm^{-1}	6.000
Reflections collected	3020
Independent reflections	2068
R(int)	0.0636
2θ range / deg	6.334 to 50.016
F(000)	418
GOF on F^2	1.023
R_1 / wR_2 [$I > 2\sigma(I)$]	0.0703/0.1277
R_1 / wR_2 (all data)	0.0953/0.1444
Largest diff. peak / hole / e $Å^{-3}$	2.27/-1.50

Table S1. The crystal data and structural refinement parameters for Tb-MOF
[a]$R_1 = \Sigma||F_0| - |F_c||/\Sigma|F_0|$. [b]$wR_2 = [\Sigma w(F_0^2 - F_c^2)^2/\Sigma w(F_0^2)^2]^{1/2}$.

Table S2. The results of spike-and-recovery experiences.

Sample	Tap Water (μM)	ADD (μM)	Found (μM)	RSD (%)	Recovery（%）
1	-	2.50	2.47	1.74	98.8
2	0.200	2.50	2.64	1.51	97.7
3	0.087	2.50	2.61	2.13	100.9

Table S3. Recent reported references related to the detection of nitrite.

Materials	Methods	Linear Range	LOD	Ref.
Cu-MOF/Au	Electrochemical	0.1 μM - 4000 μM	82.00 nM	S1
m-CDs@$[Ru(bpy)_3]^{2+}$	Fluorescent	63 nM - 2.0 μM	18.00 nM	S2
CDs-coated silica nanoparticles	Fluorescent	100 - 160 μg/L	1.00 μg/L	S3
GNRs-Azo-GNPs	Fluorescent	Up to 50 μM	0.01 μM	S4
ZnO@Ag nanosphere	SERS	0.1 nM - 1mM	0.03 nM	S5
benzo[a]phenoxazine containing o-phenylenediamine group	Fluorescent	Up to 26.0 μM	45.00 nM	S6
N-CNDs	Fluorescent	Up to 1.0 mM	1.00 μM	S7
PA	Fluorescent	0.1 μM - 10 μM	43.00 nM	S8
$\{[Ln_2Zn(abtc)_2(H_2O)_4]\cdot 2H_2O\}_\infty$	Fluorescent	-	-	S9
UiO-66-NH_2-Cit	Fluorescent	0 - 800 μM	-	S10
Rh110@MOF-801	Fluorescent	2 μM - 7 μM	0.35 μM	S11
Tb^{3+}@In-MOF	Fluorescent	0 - 70 μM	-	S12
$\{[Tb(CA)(OA)_{0.5}(H_2O)_2]\cdot H_2O\}_n$	Fluorescent	0 - 15.38 μM	28.25 nM	This work

{LOD: limit of detection; Ref.: reference; bpy: bipyridine; GNRs-Azo-GNPs: Griess reaction modulated gold nanorods (GNRs)-Azo-gold nanoparticles (GNPs); SERS: surface-enhanced Raman scattering; N-CNDs: (N)-doped carbon nanodots; PA: 2-(1H-phenanthro[9,10-d]imidazol-2-yl)aniline. Rh110: rhodamine 110}

Table S4. The lifetimes of Tb-MOF before and after adding different $NaNO_2$ with different concentrations.

C/μM	τ/μs	χ^2
0	415.56	1.086
0.666	320.49	1.158
1.329	258.09	1.185
1.990	214.52	1.150
2.649	183.29	1.145
3.306	160.96	1.132

Table S5. The linear fitting parameters of each S−V plots of Tb-MOF.

Volume (μL)	Slope (μM^{-1})	Standard Error
3	0.468	0.0039
5	0.474	0.0164
10	0.478	0.0046
Unity	0.482	0.0025

References:

S1. H. Chen, T. Yang, F. Liu and W. Li, Electrodeposition of gold nanoparticles on Cu-based metal-organic framework for the electrochemical detection of nitrite, *Sensors & Actuators: B. Chemical*, **2019**, 286, 401.

S2. Y. Zhan, Y. Zeng, L. Li, F. Luo, B. Qiu, Z. Lin and L. Guo. Ratiometric Fluorescent Hydrogel Test Kit for On-Spot Visual Detection of Nitrite, *ACS Sensor*, **2019**, 4, 1252.

S3. G. Xiang, Y. Wang, H. Zhang, H. Fan, L. Fan, L. He, X. Jiang and W. Zhao. Carbon dots based dual-emission silica nanoparticles as ratiometric fluorescent probe for nitrite determination in food samples, *Food Chemistry*, **2018**, 260, 13.

S4. D. Lia, Y. Ma, H. Duan, W. Deng and D. Li. Griess reaction-based paper strip for colorimetric/fluorescent/SERS triple sensing of nitrite. *Biosensors and Bioelectronics*, **2018**, 99, 389.

S5. J. Wang, M. M. Hassan, W. Ahmad, T. Jiao, Y. Xu, H. Li, Q. Ouyang, Z. Guo and Q. Chen. A highly structured hollow ZnO@Ag nanosphere SERS substrate for sensing traces of nitrate and nitrite species in pickled food, *Sensors & Actuators: B. Chemical*, **2019**, 285, 302.

S6. Y. Zhan, R. Sun, W. Zhu, Y. Xu and J Ge. An oxazine-based near-infrared fluorescent probe for selective in cellular imaging of exogenous nitrite, *Sensors and Actuators B*, **2017**, 240, 1283.

S7. H. Zhang, S. Kang, G. Wang, Y. Zhang and H. Zhao. Fluorescence Determination of Nitrite in Water Using Prawn-Shell Derived Nitrogen-Doped Carbon Nanodots as Fluorophores, *ACS Sensor*, **2016**, 1, 875.

S8. B. Gu, L. Huang, J. Hu, J. Liu, W. Su, X. Duan, H. Li and S. Yao. Highly selective and sensitive fluorescent probe for the detection of nitrite, *Talanta*, **2016**, 152, 155.

S9. P. Du, W. Gu and X. Liu, Highly selective luminescence sensing of nitrite and benzaldehyde based on 3d-4f heterometallic metal-organic frameworks, *Dalton Transactions*, **2016**, 45, 8700.

S10. S. Zhu, L. Zhao, B. Yan, A novel spectroscopic probe for detecting food preservative NO_2^-: Citric acid functionalized metal-organic framework and luminescence sensing, *Microchemical Journal*, **2020**, 155, 104768.

S11. C. Huang, Y. Ye, L. Zhao, Y. Li and J. Gu. One-Pot Trapping Luminescent Rhodamine 110 into the Cage of MOF-801 for Nitrite Detection in Aqueous Solution, *J. Inorg. Organomet. Polym.*, **2019**, 29, 1476.

S12. J. Wu and B. Yan. Luminescent Hybrid Tb^{3+} Functionalized Metal-Organic Frameworks Act as Food Preservative Sensor and Water Scavenger for NO_2^-, *Ind. Eng. Chem. Res.*, **2018**, 57, 7105.